Efficient coupling between a photonic crystal waveguide and a nanometer waveguide with an asymmetric resonator

2012 J. Opt. 14 055503

(http://iopscience.iop.org/2040-8986/14/5/055503)

IOP Publishing Journal of Optics A: Pure and Applied Optics
J. Opt. **14** (2012) 055503 (6pp) doi:10.1088/2040-8978/14/5/055503

Efficient coupling between a photonic crystal waveguide and a nanometer waveguide with an asymmetric resonator

Naidi Cui[1,2], Jingqiu Liang[1], Zhongzhu Liang[1], Jianwei Zhou[1,2], Bo Yang[1,2], Yongqiang Ning[1] and Weibiao Wang[1]

[1] State Key Laboratory of Applied Optics, Changchun Institute of Optics, Fine Mechanics and Physics, Chinese Academy of Sciences, Changchun, 130033, People's Republic of China
[2] Graduate School of Chinese Academy of Sciences, Beijing 100039, People's Republic of China

E-mail: wangwbt@126.com.

Received 2 June 2011, accepted for publication 4 April 2012
Published 2 May 2012
Online at stacks.iop.org/JOpt/14/055503

Abstract
A new approach to achieve efficient coupling between photonic crystals and a nanometer waveguide via an asymmetric resonator is proposed. The asymmetric resonator was composed of the photonic crystal and the nanometer waveguide was constructed by elongating a rod of the photonic crystal resonator horizontally. By introducing the asymmetric resonator, the nanometer waveguide served as a part of the resonator, and the coupling between the photonic crystal waveguide and the nanometer waveguide was converted to internal coupling between the photonic crystal devices. The 3D theoretical coupling efficiency reached 91.31%. Such compact, efficient coupling shows great promise for applications in molecular imaging, nanoprobes, integrated photonic circuits and on-chip optical interconnects.

Keywords: photonic crystals, nanometer waveguide, resonator, photonic integrated circuits

(Some figures may appear in colour only in the online journal)

1. Introduction

Photonic crystals (PCs) are envisaged as the main candidates for the implementation of future integrated photonic/optical circuits because of their compact structure and appealing optical functionalities. Central to the appeal of utilizing photonic crystals for nanophotonic and optical applications is their ability to control the flow of light, enabling functionalities such as guiding the light with a line defect [1–3] and restraining the light in an ultra-small volume with a point defect [4–6]. Two-dimensional rod based PCs are powerful tools for characterizing emitting applications such as light emitting diodes (LEDs) [7, 8], but fabrication of high aspect ratio rods is a major challenge. However, with recent advances in the synthesis of semiconducting nanowires through controlled vapor–liquid–solid growth (VLS) [9, 10] via atomic force microscopy (AFM), it is timely to begin integrating nanowires to construct high aspect ratio 2D rod based PC functional devices. The key point of VLS-based PCs is control of the size and the lattice of the catalyst seed particles. Nano-manipulation of the catalyst seed particles is one potential method [11]. Måttensson also reported 2D PC structures fabricated through VLS with nanoimprint techniques to control the size and the lattice of the catalyst seed particles [12]. Additionally, high aspect ratio nanorods or nanowires can also be fabricated through reactive ion etching with improved holographic lithography [13] or block copolymer lithography [14].

By virtue of their compact structure and extremely small diameter, semiconducting nanometer waveguides (NWGs) are ideally suited for ultracompact photonics devices. Thus, efficient coupling between PCs and NWGs is an issue of significant value due to the potential applications of the integrated optical circuit. Some works have achieved efficient coupling from rib waveguides to PCs through the slow mode [15, 16], Bloch mode [17], resonant mode [18] and

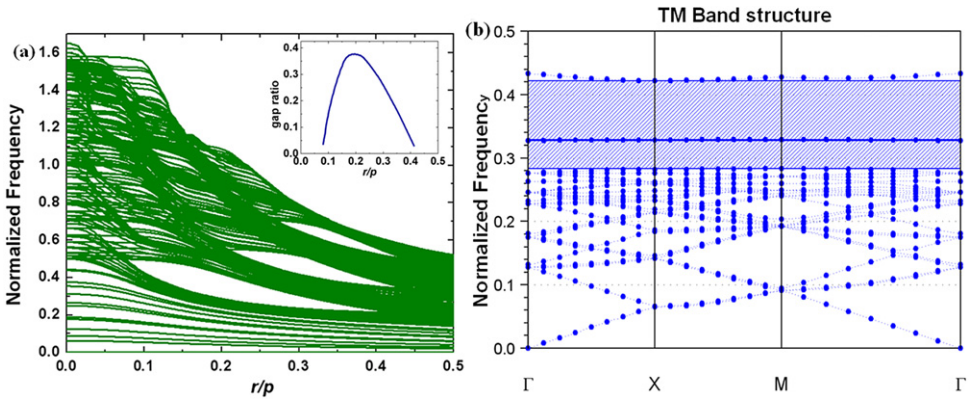

Figure 1. The photonic band characteristics of the PCs. (a) The photonic crystal gap of the rod-based PCs as a function of the filling rate. (b) The defect mode of the PC resonator with a point defect of $r_p = 0.1$, $p = 0.051$ μm when the filling rate is 0.2.

tapered structure [18]. However, there is little work about the coupling of PCs and NWGs. Unlike these works, we elongated a rod of the resonator horizontally to construct the NWG. The NWG served as part of the resonator, and the resonator that was composed of a PC and an NWG was termed an asymmetric resonator. The introduction of the asymmetric resonator converted the PC waveguide (PCWG)–NWG coupling to internal coupling of PC devices (PCWG–PC resonator coupling), which simplified the design and optimization of the structure.

Efficient coupling of the PCWG and the NWG combines the PC devices and traditional optical components together, and has advantages in optoelectronic based applications, such as molecular imaging, nanoprobes, and on-chip optical interconnects.

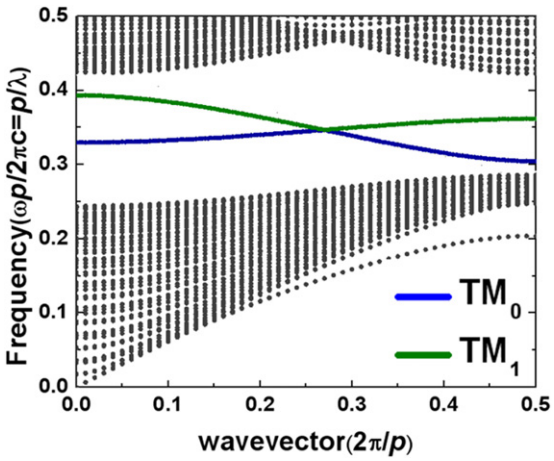

Figure 2. The dispersion curve of the PCWG with a line defect of 0.165 μm.

2. 2D theoretical discussion

In this paper, we designed the PC structure on 2D rod-based PCs. Serving as a connecting device, the lattice period was set to 0.51 μm to integrate with the PC devices in the optical circuits we designed.

The appropriated photonic crystal band gap (PBG), especially the PBG located between the first and second bands, is important in the design of PBG-based PC devices. Figure 1(a) shows the three photonic bands of the silicon rod based PCs. Herein, we define the gap ratio as the width of the first photonic band gap divided by that of the whole band, as shown in the inset of the figure 1(a). The gap ratio shows the occupancy of the PBG in the whole band. When r/p is 0.2 ($r = 0.2p = 0.102$ μm), the gap ratio reaches the maximum value. Figure 1(b) shows the defect mode of the point defect with radius $r_p = 0.1p = 0.051$ μm, when the filling rate is 0.2. A resonance mode with a normalized frequency of 0.329 is obtained. Dependent on the definition of the normalized frequency, $F = \omega a/2\pi c = a/\lambda$, the calculated selecting wavelength is 1550 nm, which fulfils the design requirement.

To achieve efficient coupling of the PCWG and the PC resonator, we should set the selecting wavelength of PC waveguide to 1550 nm too. Introduction of a line defect by omitting a row of rods is a useful method for constructing the PCWG. However, the out-of-plane loss in this type of PCWG influences the performance of the 2D PC waveguide dramatically. An effective approach to restrain the out-of-plane loss of the dielectric rod based PCWG is introduction of a line defect with a radius different from that of the surrounding PC slab, instead of introducing the missing rods [19]. Figure 2 shows the dispersion curves of a PC waveguide that was constructed by introducing a line defect with a radius of $r_1 = 0.165$ μm. Unlike a PCWG with a missing row, this PCWG generates two modes: TM_0 and TM_1. However, this PCWG has low loss too. We simulated the transmission characteristics and found that the PC waveguide works effectively (only 0.02 db in 20 μm length at a wavelength of 1550 nm).

A schematic of the structure of the coupling system is shown in figure 3. In this paper, we intend to find a novel coupling structure to realize efficient coupling between the PCWG and the NWG. There are some difficulties due to the different widths of the PCWG and the NWG. Because of its ultra-small volume and the ultra-concentrated light, the PC resonator provides a new approach to realize efficient coupling. Normally, a PC resonator is constructed with 5×5

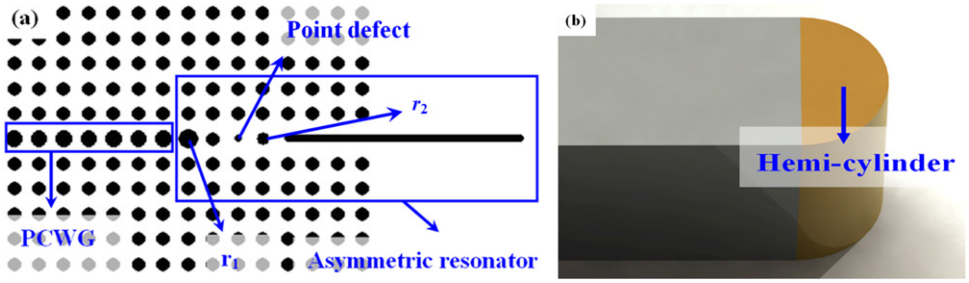

Figure 3. The structure of the coupling system with a hemi-cylinder tipped NWG. (a) Schematic of the coupling system. (b) The hemi-cylinder tipped NWG.

arrays. As shown in figure 1(a), a silicon rod located at the edge of the resonator is elongated horizontally to construct the NWG. The two ends of the NWG are hemi-cylinders, as shown in figure 3(b). The NWG is a part of the asymmetric resonator, and, at the same time, it is set as the output channel of the coupling system. The length of the NWG was set to 3.06 μm. The resonator is composed of PCs and an NWG. Thus, we call it an asymmetric resonator. The PCWG–NWG coupling was converted to the internal coupling of the PC devices (the coupling between PCWG and the PC asymmetric resonator). The coupling efficiency was sensitive to the radius of the rod located at the interface of the PCWG and the NWG (r_1) and the width of the NWG. These parameters will be optimized in section 3. The radii of all the rods except r_1 were 0.102 μm.

The optical performance of the PC resonator based device is determined by the quality of the PC resonator. For an appropriately designed resonator and sufficiently large surrounding photonic crystal material, the intrinsic loss of the cavity is attributed to the reflection loss at the interface between the interior and exterior of the cavity [20–22]. The quality of the 2D PC resonator is influenced by the out-of-plane loss of the lightwaves. One of the best approaches to resolve this problem is the PC slab or air-bridge structure, in which the lightwaves are confined by total internal reflection at the interface between the substrate and the air cladding in the vertical direction [23, 24]. Herein, the relevant structure parameters were realistically estimated in silicon-on-insulator (SOI) to construct the PC slab structure. We located the source inside the structure because the input coupling issue was outside of the scope of the paper.

The NWG served as a part of the asymmetric resonator. Therefore, the efficient coupling of the PCWG and the NWG was converted to the internal coupling of the PCWG and the asymmetric resonator. Efficient coupling can be obtained by optimizing the structure parameters of the asymmetric resonator. Figure 4(a) shows the dispersion relation of the coupling system. The white regions indicate wavelengths where propagation into the photonic crystal is forbidden. Propagation into the photonic crystal is only possible for the wavelengths denoted by the points. Modes in the upper section of the light line will cause out-of-plane scattering losses because the effective index for modes located above the light line is smaller than that of the substrate. By introducing the asymmetric PC resonator, the PCWG–NWG coupling is converted to PCWG–PC resonator coupling. Therefore, we only need to analyze the dispersion relation of the PCWG and the asymmetric resonator. The PCWG generates two modes: TM_0 and TM_1. The anti-crossing of the TM_0 and TM_1 modes is shown in figure 4(b), and leads to a mini-bandgap [25]. At the anti-crossing point, the TM_0 mode changes from odd to even and the TM_1 mode changes from even to odd, as shown in figure 4(c). The I and III parts of figure 4(c) are the TM_0 and TM_1 modes before the anti-crossing point. The II and IV parts are the TM_0 and TM_1 modes after the anti-crossing point. As illustrated in figure 4(a), the PC's asymmetric resonator dispersion curve crosses part II (the TM_0 mode after the anti-crossing point) at point B, where the selecting wavelength is about 1.55 μm. The intersection point was used to realize efficient coupling between the PCWG and the asymmetric resonator, as there the lightwaves of the selecting wavelength can couple from the PCWG to the PC asymmetric resonator without mode-mismatch loss.

As part of the resonator, the NWG replaces the rod located at the edge of the resonator and acts as the output channel. The lightwaves coupled out from the resonator are influenced by the parameters of the NWG. Herein, the NWG is designed with two hemi-cylindered tips. NWGs constructed with left or right hemi-cylinder tips are also shown in figure 5(a). The right and left directions in figure 5(a) are analogous to those in figure 3(a).

The parameters of the elements surrounding the point defect determine the performance of the coupling system. Figure 5(b) reveals the curves of the coupling efficiency as a function of the width of the NWG. The coupling efficiency is above 95% for a wide range of w of about 60 nm (ranges from 0.083 to 0.147 μm, about 60 nm wide). If we decrease our requirement on the coupling efficiency to 90%, the efficient region ranges from 0.063 to 0.15 μm, which is nearly 90 nm wide. NWGs with widths of around 100 nm have attracted a lot of interest [26–28]. Therefore, the design in this paper provides a large fabrication tolerance.

To enhance the coupling efficiency, the key point is to decrease the reflection loss that is determined by the radius of the rod located between the PCWG and the PC resonator (r_1), as shown in figure 3(a). Figure 5(c) reveals the normalized intensities of the output beams for the four types of NWG as a function of r_1. Among the four types of NWG, the NWG with two hemi-cylindered tips is the most efficient one, extremely so for the main peak. The

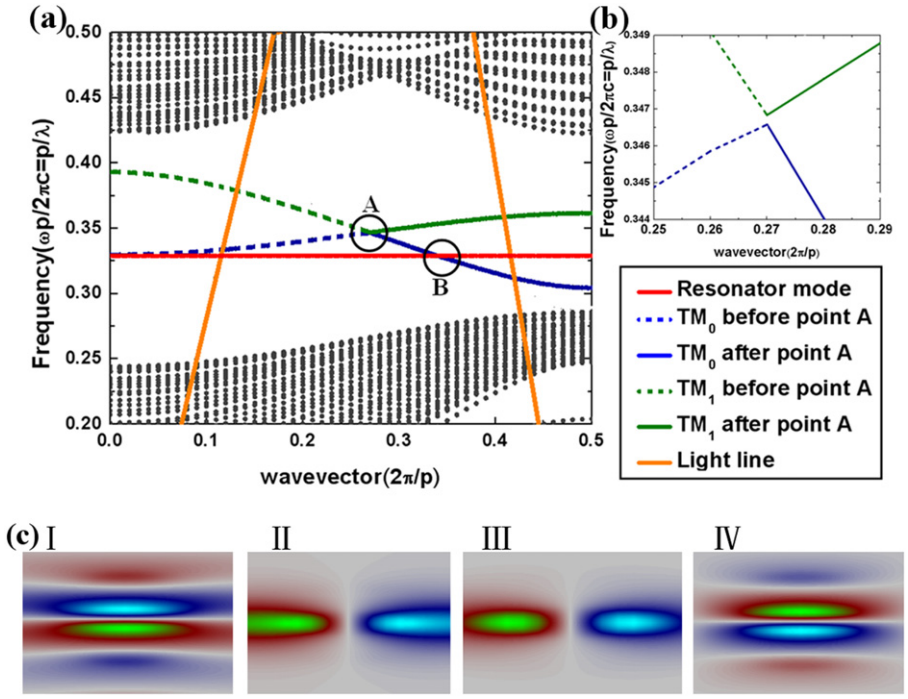

Figure 4. (a) Dispersion curves of the PCWG and the PC resonator. As denoted by the B point, the dispersion curves of the PCWG and the PC resonator intersect when the normalized frequency is 0.329. (b) A detailed view of the mini-bandgap. (c) The field patterns of the modes of the PCWG. Parts I and II of figure 4(c) are related to the TM_0 modes before and after point B respectively. Parts III and IV are related to the TM_1 modes before and after point B respectively.

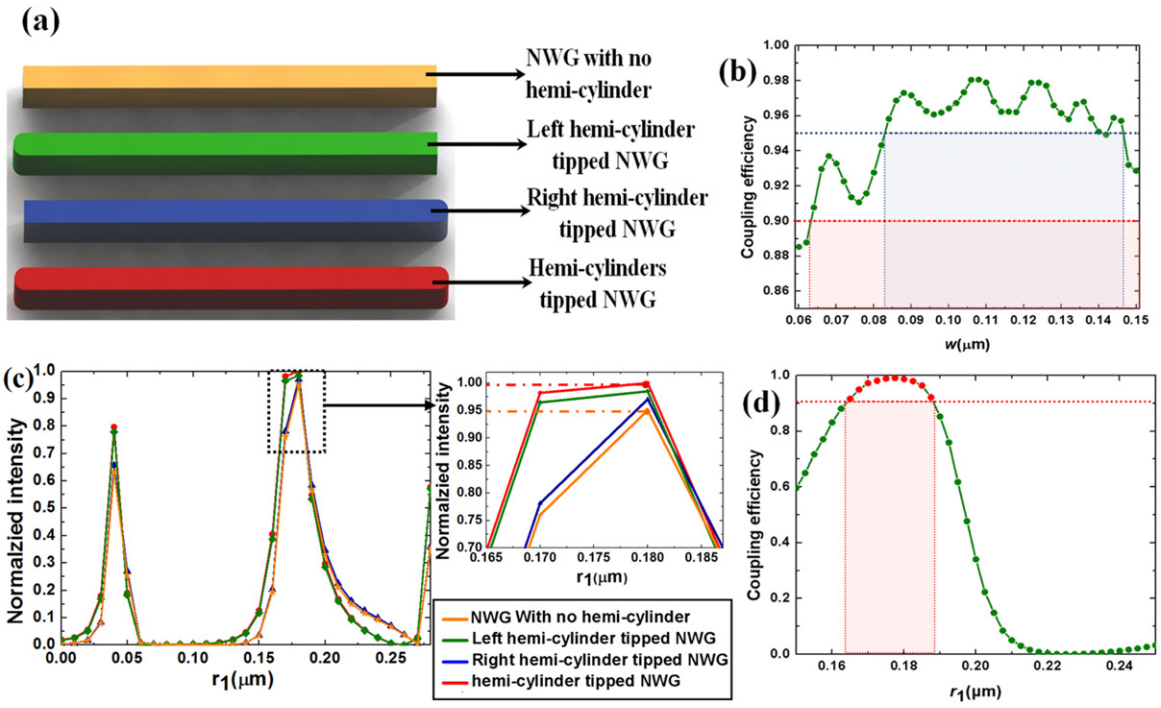

Figure 5. The coupling efficiency of the coupling system. (a) A schematic of the structures of the four types of NWG. (b) The curves of the coupling efficiency versus the width of the NWG. (c) The normalized intensity of the output beam for the four types of NWG as a function of r_1. (d) The coupling efficiency as a function of r_1.

NWG constructed with no hemi-cylinders provides the lowest intensity of the output beam. In addition, the hemi-cylinder tipped NWG has potential applications in molecular imaging and nanoprobes [29, 30]. Figure 5(d) reveals the coupling efficiency as a function of the value of r_1. $r_1 = 0.18$ μm was selected where the coupling efficiency is about 98.64%. The

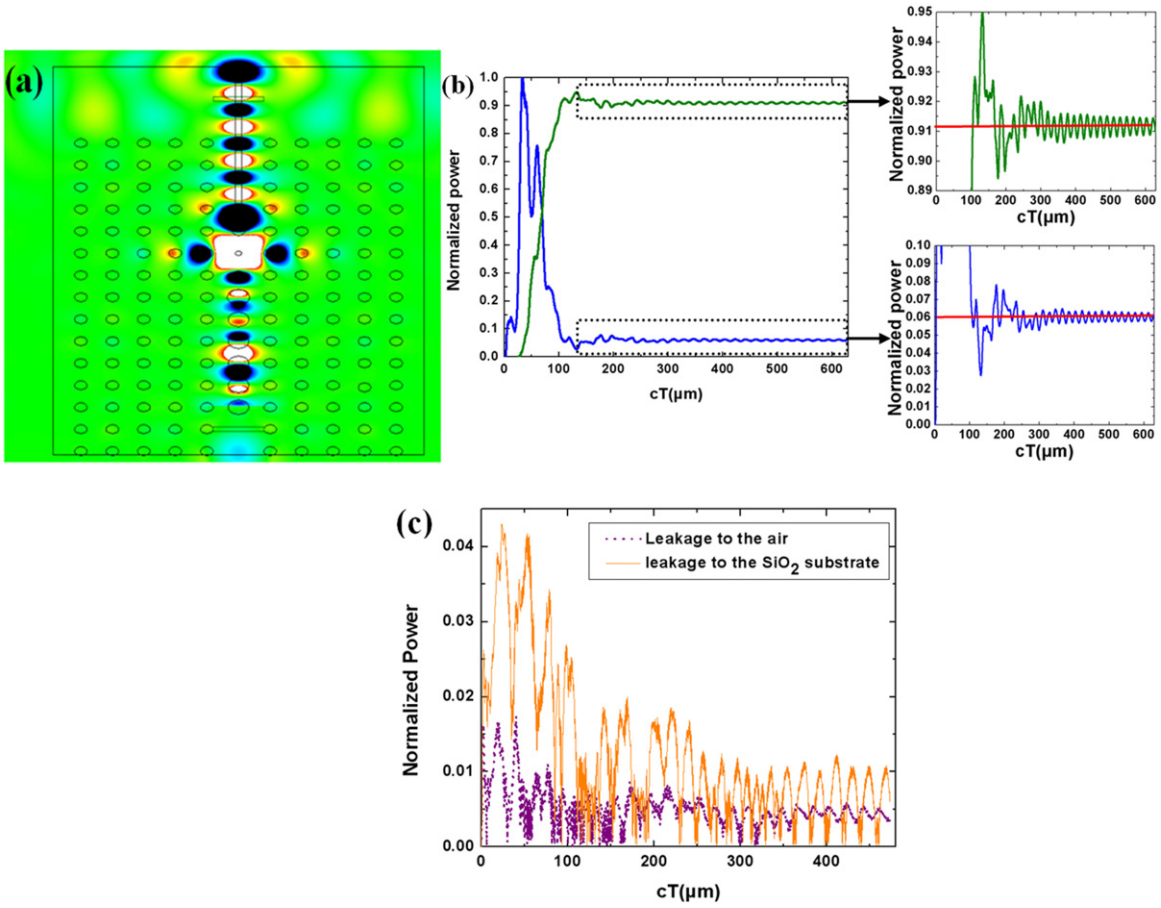

Figure 6. The 3D analysis of the coupling system. (a) The field pattern of the coupling system calculated with 3D FDTD. (b) The space-domain of the intensity of the output beam and the reflection loss. (c) The leakage of the coupling system.

coupling system provides a coupling efficiency higher than 90% for a wide range of more than 20 nm of r_1 that ranges from 0.165 to 0.185 μm (denoted by red points).

The main parameters optimized in this paper are w and r_1. As depicted in figures 5(a) and (b), wide selections of about 90 nm and 20 nm for w and r_1 respectively are provided. In this paper, the width of the NWG $w = 0.105$ μm is selected, where the coupling efficiency reached the maximum value. For a value of w that is not in the efficient region, we can optimize the parameters of the coupling system to gain efficient coupling, especially the parameters of the rods around the point defect. For example, the coupling structure can realize efficient coupling (about 93%) between the PCWG and the NWG with a width of 200 nm when $r_1 = 0.225$ μm, $r_2 = 0.06$ μm.

3. 3D investigation

The above theoretical analysis is based on the 2D FDTD technique that corresponds to infinitely long rods. For realistic aspects of 2D PC devices, the height of the device is finite. The 2D FDTD calculation can provide theoretical guidance and save design time; however, it is not accurate enough. To check the applicability of the design, we verified the coupling system with the 3D FDTD solution. The heights of the rods and the NWG are set to 7.65 μm and the buried SiO_2 layer is set to 3 μm; these values are sufficient to restrain the vertical loss [31].

Figure 6(a) shows the field pattern of the coupling system calculated with the 3D FDTD technique. Through the coupling of the PC asymmetric resonator, efficient coupling of the PCWG and the NWG is realized. Figure 6(b) reveals the power value of the output beam and the reflection loss as a function of time. The curves act as damping-like vibration and fluctuate around an average value when $cT >$ 300 μm (marked with a dashed rectangle in the insets). The average value of the output beam is around 0.9131. The coupling efficiency is about 91.31%. Similarly, the average reflection loss is about 0.06. The out-of-plane loss is shown in figure 6(c). Since the index contrast of the substrate and the rods is smaller than that of the air and the rods, the leakage to the substrate is larger. The total leakage losses are 0.012. The other power loss (about 0.0149) mainly comes from the transmission losses. The 3D calculated coupling efficiency is a little lower than that calculated with the 2D FDTD technique (98.64%). It has been demonstrated that the efficiency of resonator based PC devices is influenced by the Q-factor. The Q-factor is determined by the height of the rods [25]. The decrease of the coupling efficiency mainly comes from the decrease of the Q-factor of the resonator

when calculated with 3D technology. The Q-factor of the 3D calculation approaches the result of its 2D counterpart on increasing the height of the rods. When the height of the rods is infinite, the 3D calculation is equal to the 2D calculation. Additionally, the leakage from the substrate and air is ignored in the 2D calculation because of the intrinsic characteristic of the 2D technique. However, when calculated with the 3D solution, the vertical loss cannot be entirely restrained even through low refractive index materials are deposited on the top and the bottom (air and SiO_2 respectively). The 3D calculation confirms the applicability of the design that performed with 2D FDTD.

4. Conclusion

By introducing the PC asymmetric resonator, the coupling between the PCWG and the NWG was converted to coupling between the PCWG and the PC asymmetric resonator, which gave a more compact structure and made the design and the optimization easier. A hemi-cylinder tipped NWG with a radius of 0.105 μm and length of 3.06 μm served as part of the resonator. The theoretical calculation demonstrated that the hemi-cylinder tipped NWG was more efficient. The 2D coupling efficiency reached 98.64% when r_1 was set to 0.18 μm. The PCWG–NWG coupling system was verified with the 3D technique. The 3D coupling efficiency was about 91.31%. The decrease of the coupling efficiency mainly comes from the decrease of the Q-factor. This efficient coupling can be widely used in molecular imaging, nanoprobes, and on-chip optical interconnects.

Acknowledgment

This work was supported by the National Natural Science Foundation of China (Grant No 60877031).

References

[1] Jun-Ichiro S, Noritsugu Y, Makoto O, Kazuhiro K, Toyohiko Y and Masahide I 2008 *Opt. Commun.* **281** 5788
[2] Cui N, Liang J, Liang Z, Zhou J, Ning Y and Wang W 2010 *Opt. Precis. Eng.* **18** 2549
[3] Tada T, Poborchii V V and Kanayama T 2002 *Microelectron. Eng.* **63** 259
[4] Xu G, Colombelli R, Braive R, Beaudoin G, Le Gratiet L, Talneau A, Ferlazzo L and Sagnes I 2010 *Opt. Express* **18** 11979
[5] Nomura M, Ota Y, Kumagai N, Iwamoto S and Arakawa Y 2010 *Appl. Phys. Lett.* **97** 191108
[6] Safavi-Naeini A H, Mayer Alegre T P, Winger M and Painter O 2010 *Appl. Phys. Lett.* **97** 181106
[7] Matioli E and Weisbuch C 2010 *J. Phys. D: Appl. Phys.* **43** 354005
[8] Cho C-Y, Kang S-E, Kim K S, Lee S-J, Choi Y-S, Han S-H, Jung G-Y and Park S-J 2010 *Appl. Phys. Lett.* **96** 181110
[9] Hannon J B, Kodambaka S, Ross F M and Tromp R M 2006 *Nature* **440** 69
[10] Wu Z H, Sun M, Mei X Y and Ruda H E 2004 *Appl. Phys. Lett.* **85** 657
[11] Ohlsson B J, Björk M T, Magnusson M H, Deppert K and Samuelson L 2001 *Appl. Phys. Lett.* **79** 3335–8
[12] Måttensson T, Carlberg P, Borgström M, Montrlius L, Seifert W and Samuelson L 2004 *Nano Lett.* **4** 699–702
[13] Hung Y-Jr, Lee S-L, Thibeault B J and Coldren L A 2010 *Mater. Res. Soc. Symp. Proc.* **1258** Q14–02
[14] Zschech D, Kim D H, Milenin A P, Scholz R, Hillebrand R, Kawker C J, Russell T P, Steinhart M and Gösele U 2007 *Nano Lett.* **7** 1516–20
[15] Velha P, Hugonin J P and Lalanne P 2007 *Opt. Express* **15** 6102
[16] Vlasov Y A and McNab S J 2006 *Opt. Lett.* **31** 50
[17] Momeni B and Adibi A 2005 *Appl. Phys. Lett.* **87** 171104
[18] Scullion M G, Krauss T F and Di Falco A 2011 *IEEE Photon. J.* **3** 203
[19] Assefa S, Rakich P T, Bienstman P, Johnson S G, Petrich G S, Joannopoulos J D, Kolodziejski L A, Ippen E P and Smith H I 2004 *Appl. Phys. Lett.* **85** 6110
[20] Nanaee M G and Young J F 2008 *Opt. Express* **16** 20908
[21] Akahane Y, Asano T, Song B S and Noda S 2003 *Nature* **425** 944
[22] Faraon A, Waks E, Englund D, Fushman I and Vuckovic J 2007 *Appl. Phys. Lett.* **90** 073102
[23] Kawai N, Inoue K, Carlsson N, Ikeda N, Sugimoto Y, Asakawa K and Takemori T 2001 *Phys. Rev. Lett.* **86** 2289
[24] Qiu M 2002 *Phys. Rev.* B **66** 033103
[25] Olivier S, Benisty H, Weisbuch C, Smith C J M, Krauss T F and Houdré R 2003 *Opt. Express* **11** 1490
[26] Van Vugt L K, Piccione B and Agarwal R 2010 Incorporating polaritonic effects in semiconductor nanowire waveguide dispersion *Appl. Phys. Lett.* **97** 061115
[27] Van Vugt L K, Zhang B, Piccione B, Spector A A and Agarwal R 2009 Size-dependent waveguide dispersion in nanowire optical cavities: slowed light and dispersionless guiding *Nano Lett.* **9** 1484–688
[28] Huang Y J, Lu W T and Sridhar S 2008 Nanowire waveguide made from extremely anisotropic metamaterials *Phys. Rev.* A **77** 063836
[29] Malcolm N P, Heltzel A J, Sokolov K V, Shi L and Howell J R 2008 *Appl. Phys. Lett.* **93** 193101
[30] Heltzel A J, Shi L and Howell J R 2011 *Nanotechnology* **22** 045203
[31] Xu T, Yang S, Nair S V and Ruda H E 2007 *Phys. Rev.* B **75** 125104